

$SE(3)$ -Based Trajectory Optimization and Target Tracking in UAV-Enabled ISAC Systems

Dongxiao Xu*, Xinyang Li*, Vlad C. Andrei*, Moritz Wiese*, Ullrich J. Mönich*, Holger Boche*

*Chair of Theoretical Information Technology

Technical University of Munich

Munich, Germany

Emails: {dongxiao.xu, xinyang.li, vlad.andrei, wiese, moenich, boche}@tum.de

Abstract—This paper introduces a novel approach to enhance the performance of UAV-enabled integrated sensing and communication (ISAC) systems. By integrating uniform planar arrays (UPAs) and modeling the UAV as a rigid body using $SE(3)$, the study addresses key challenges in existing ISAC frameworks, such as rigid-body dynamics and trajectory design. We propose a target tracking scheme based on extended Kalman filtering (EKF) in $SE(3)$ and trajectory optimization from a control signal design perspective, leveraging the conditional Posterior Cramer-Rao bound (CPCRB) to optimize performance. Numerical results demonstrate the effectiveness of the proposed method in improving target tracking and trajectory optimization for a UAV-enabled MIMO-OFDM ISAC system.

I. INTRODUCTION

Unmanned aerial vehicles (UAVs), serving as aerial base stations (BS), are expected to revolutionise the integrated sensing and communication (ISAC) systems with their high mobility and flexible deployment. Recent research has focused intensively on the joint beamforming and UAV trajectory optimisation for ISAC [1], [2], yet key limitations remain.

(i) **Antenna Array Limitations:** Many prior works either do not specify antenna arrays [3], [4], or assume uniform linear arrays (ULA), mounted vertically [2] or horizontally [1]. However, ULAs capture only one degree of freedom for angles of arrival (AoA) or departure (AoD), restricting their sensing ability in 3D space. In contrast, uniform planar arrays (UPA) inherently support 3D spatial relationships and enhance sensing capabilities. (ii) **Rigid-Body Dynamics:** Most prior works [5] assume static ground users (GUs) or sensing targets, while others [3] focus on moving target tracking and real-time trajectory design for multi-UAVs in SISO settings. The adoption of UPAs, however, necessitates modeling UAV as a rigid body, where the Lie group $SE(3)$ effectively captures spatial displacement and orientation dynamics. (iii) **Trajectory Design Challenges:** Trajectories, typically as sequences of future states and actions, are often explored in dynamic programming (DP) or model predictive control (MPC). However, state-of-the-art methods [3] primarily focus on optimizing UAV positions while overlooking control design aspects, which are crucial for practical implementation. (iv) **Posterior Cramer-Rao Bound (PCRB):** While PCRB is used to quantify estimation accuracy, prior works focus on optimizing power and bandwidth [6], beamforming [7], [8],

or waveform design [9], limited number of works consider trajectory optimization based on PCRB metrics.

This work addresses these limitations by proposing a novel approach for a UAV-enabled MIMO-OFDM ISAC system that incorporates UPA configurations and rigid-body dynamics via $SE(3)$, enabling target tracking as well as trajectory design from a control perspective.

II. SYSTEM MODEL

A. Radar Signal Model

Considering a MIMO-OFDM ISAC system, where the UAV is equipped with a half wavelength spacing UPA with N_T and N_R antennas. The steering vector of the UPA is expressed as

$$\mathbf{a}(\theta, \phi) = \mathbf{a}_y(\theta, \phi) \otimes \mathbf{a}_x(\theta, \phi) \in \mathbb{C}^N, \quad (1)$$

$$\mathbf{a}_x(\theta, \phi) = \frac{1}{\sqrt{N_x}} [1, -e^{j\pi \sin \theta \cos \phi}, \dots, -e^{j\pi(N_x-1) \sin \theta \cos \phi}]^T, \quad (2)$$

$$\mathbf{a}_y(\theta, \phi) = \frac{1}{\sqrt{N_y}} [1, -e^{j\pi \sin \theta \sin \phi}, \dots, -e^{j\pi(N_y-1) \sin \theta \sin \phi}]^T, \quad (3)$$

where \otimes indicates the kronecker product, θ and ϕ the polar angle and azimuthal angle, respectively, and $N = N_x N_y$. The Tx and Rx array responses share the same structure, i.e., $\mathbf{a}_T(\theta, \phi) = \mathbf{a}_{T,y}(\theta, \phi) \otimes \mathbf{a}_{T,x}(\theta, \phi) \in \mathbb{C}^{N_T}$, and $\mathbf{a}_R(\theta, \phi) = \mathbf{a}_{R,y}(\theta, \phi) \otimes \mathbf{a}_{R,x}(\theta, \phi) \in \mathbb{C}^{N_R}$, where $N_T = N_{T,x} N_{T,y}$, $N_R = N_{R,x} N_{R,y}$. The UAV communicates with a single GU while performing sensing by collecting signals reflected from the GU, serving as a mono-static radar. Thus, AoA approximates AoD. Assuming a single line-of-sight (LOS) path, the channel frequency response at subcarrier ℓ and OFDM symbol k is given as

$$\mathbf{H}_{\ell,k} = b \cdot \omega_{\ell,k} \cdot \mathbf{a}_R(\theta, \phi) \mathbf{a}_T(\theta, \phi)^H, \quad (4)$$

with $\omega_{\ell,k} = e^{-j2\pi\ell f_0\tau} e^{j2\pi\mu k T_s}$, where

- $T_s = 1/f_0 + T_g$ is the OFDM symbol duration, with T_g the cyclic prefix duration, f_0 the subcarrier spacing,
- τ is the path delay,
- μ is the doppler shift due to mobilities,
- $\mathbf{a}_T(\theta, \phi) \in \mathbb{C}^{N_T}$ is the UPA response at AoD θ, ϕ ,
- $\mathbf{a}_R(\theta, \phi) \in \mathbb{C}^{N_R}$ is the UPA response at AoA θ, ϕ ,
- $b \in \mathbb{C}$ is the LOS-channel gain, which comprises the amplitude attenuation and phase shift, i.e., $b = |b| \cdot e^{j\varphi} = a \cdot d^{-2} \cdot e^{j\varphi}$, where $a \triangleq \sqrt{\frac{\lambda_c^2 \sigma_{\text{RCS}}}{(4\pi)^3}} \in \mathbb{R}$, with σ_{RCS} the radar cross section (RCS), λ_c the wavelength of the

centre frequency f_c . Strictly speaking, the phase shift φ depends on the path delay [10], but for $d \gg \lambda_c$, it can be considered as a uniformly distributed random variable [11], i.e., $\varphi \sim \mathcal{U}(-\pi, \pi)$.

Suppose the UAV transmits a signal $\mathbf{x}_{\ell,k}$ at the (ℓ, k) -th OFDM resource element (RE) of size $L \times K$. The reflected signal received at the UAV is $\mathbf{y}_{\ell,k} = \mathbf{H}_{\ell,k} \mathbf{x}_{\ell,k} + \mathbf{z}_{\ell,k}$, with $\mathbf{z}_{\ell,k} \in \mathbb{C}^{N_R}$ being the additive gaussian noise of zero mean and covariance matrix $\mathbf{C}_{\mathbf{z}_{\ell,k}} = \sigma_z^2 \mathbf{I}_{N_R}$, i.e., the noise on different receive antennas is assumed to be independent. By using the property of the kronecker product, we have $\mathbf{y}_{\ell,k} = (\mathbf{x}_{\ell,k}^\top \otimes \mathbf{I}_{N_R}) \mathbf{h}_{\ell,k} + \mathbf{z}_{\ell,k}$, where $\mathbf{h}_{\ell,k} \triangleq \text{vec}(\mathbf{H}_{\ell,k}) = b \cdot \omega_{\ell,k} \cdot \mathbf{a}_T^*(\theta, \phi) \otimes \mathbf{a}_R(\theta, \phi)$. Without loss of generality, the sensing symbols are allocated on M OFDM REs, i.e., $\{(\ell_m, k_m)\}_{m=1}^M$. For simplicity, the subscript m is used to represent (ℓ_m, k_m) . All M received symbols can be further stacked vertically, i.e., $\mathbf{y} \triangleq [\mathbf{y}_1^\top, \dots, \mathbf{y}_M^\top]^\top = (\mathbf{X} \otimes \mathbf{I}_{N_R}) \cdot \mathbf{h} + \mathbf{z}$, with $\mathbf{X} \triangleq \text{blkdiag}(\mathbf{x}_1^\top, \dots, \mathbf{x}_M^\top) \in \mathbb{C}^{M \times MN_T}$, $\mathbf{h} \triangleq [\mathbf{h}_1^\top, \dots, \mathbf{h}_M^\top]^\top \in \mathbb{C}^{MN_R N_T}$, and $\mathbf{z} \triangleq [\mathbf{z}_1^\top, \dots, \mathbf{z}_M^\top]^\top \in \mathbb{C}^{MN_R}$, assuming independent noise on different REs, i.e., $\mathbf{C}_z = \sigma_z^2 \mathbf{I}_{MN_R}$. Besides, \mathbf{h} has a compact form given as $\mathbf{h} = b \cdot \omega \otimes \mathbf{a}_T^*(\theta, \phi) \otimes \mathbf{a}_R(\theta, \phi)$, with $\omega \triangleq [\omega_1, \dots, \omega_M]^\top \in \mathbb{C}^M$, and $\omega_m = e^{-j2\pi\ell_m f_0 \tau} e^{j2\pi\mu k_m T_s}$. The channel dependence on the physical parameters is expressed as $\mathbf{h}(\zeta)$, where $\zeta = [\tau, \mu, \phi, \theta]^\top$ as collection of all physical parameters.

B. State Evolution Model

Hereby, we treat the spatial configuration of the GU relative to the UAV as the state variable, as the *special Euclidean group* $SE(3)$ provides an ideal framework for representing rigid-body motions, comprising both rotation \mathbf{R} and translation \mathbf{r} . One element of $SE(3)$ can be expressed in the form of the *homogeneous transformation matrix* [12], i.e., $\mathbf{T} \triangleq (\mathbf{R}, \mathbf{r})$, for brevity. In this work, we consider one stationary *global frame* $\{w\}$ attached arbitrarily to the ground in an open 3D space. The UAV is modeled as a *rigid body* with an associated *body frame* $\{s\}$ located at its rotation center; while the GU is treated as a point with an attached body frame $\{p\}$ at its center.

We use the following notations: (i) $\mathbf{T}_{w,s}^n$: the configuration of the UAV's body frame $\{s_n\}$ relative to the global frame $\{w\}$ at the n -th epoch, (ii) $\mathbf{T}_{w,p}^n$: the configuration of the GU's body frame $\{p_n\}$ relative to the global frame $\{w\}$ the n -th epoch, and (iii) $\mathbf{T}_{s,p}^n$: the configuration of the GU's body frame $\{p_n\}$ relative to the UAV's body frame $\{s_n\}$ at the n -th epoch, which is expressed as $\mathbf{T}_{s,p}^n = \mathbf{T}_{s,w}^n \mathbf{T}_{w,p}^n = (\mathbf{T}_{w,s}^n)^{-1} \mathbf{T}_{w,p}^n$. The configurations $\mathbf{T}_{w,s}^n$ and $\mathbf{T}_{w,p}^n$ evolve according to the rigid-body motions of the UAV and the GU, respectively, i.e.,

$$\begin{aligned} \mathbf{T}_{w,s}^n &= \mathbf{T}_{w,s}^{n-1} \cdot \text{Exp}(\mathcal{B}\xi_s^n \Delta t) = \text{Exp}(\mathcal{E}\xi_s^n \Delta t) \cdot \mathbf{T}_{w,s}^{n-1}, \\ \mathbf{T}_{w,p}^n &= \mathbf{T}_{w,p}^{n-1} \cdot \text{Exp}(\mathcal{B}\xi_p^n \Delta t) = \text{Exp}(\mathcal{E}\xi_p^n \Delta t) \cdot \mathbf{T}_{w,p}^{n-1}, \\ \mathcal{B}\xi_p^n &= [\mathcal{B}\nu_p^{n,\top}, \mathbf{0}^\top]^\top, \quad \mathcal{B}\xi_s^n = [\mathcal{B}\nu_s^{n,\top} \quad \mathcal{B}\omega_s^{n,\top}]^\top \in \mathbb{R}^6, \end{aligned}$$

where, in general, $\mathcal{E}\mathbf{v}$ denotes the tangent element at the identity element \mathcal{E} of the $SE(3)$ group, expressed in the *spatial* or *global* frame \mathcal{E} . It corresponds to the transformed

element $\mathcal{B}\mathbf{v}$ via the *adjoint action* [13], represented in the *body* frame \mathcal{B} . In this work, the terminology of w and \mathcal{E} are used interchangeably. $\text{Exp}(\cdot)$ indicates the *capitalized exponential map* [14], which maps a vector element \mathbf{v} , as an isomorphism to the element \mathbf{v}^\wedge of the Lie algebra $se(3)$, to an element of the $SE(3)$ group, where $(\cdot)^\wedge$ denotes the *hat operator*. The Lie algebra velocity \mathbf{v}^\wedge of $SE(3)$ is known as the *twist* ξ^\wedge , which represents the motion velocity in terms of both *linear* ν and *angular velocity* ω . Naturally, we have the *spatial twist* and *body twist* as $\mathcal{E}\xi$ and $\mathcal{B}\xi$, respectively. For more details on the Lie group $SE(3)$ and its Lie algebra $se(3)$, please refer to the Appendix.

In our case, the body twist $\mathcal{B}\xi_s^n$ consists of the linear and angular velocities, i.e., $\mathcal{B}\nu_s^n, \mathcal{B}\omega_s^n \in \mathbb{R}^3$, of the UAV at the $n-1$ -th epoch, corresponding to a tangent vector at $\mathbf{T}_{w,s}^{n-1}$, i.e., $\mathcal{B}\xi_s^n \in T_{\mathbf{T}_{w,s}^{n-1}} SE(3)$; while $\mathcal{B}\xi_p^n$, comprising the linear velocity, i.e., $\mathcal{B}\nu_p^n \in \mathbb{R}^3$, and zero angular velocity of the GU at the $n-1$ -th epoch, corresponds to a tangent vector at $\mathbf{T}_{w,p}^{n-1}$, i.e., $\mathcal{B}\xi_p^n \in T_{\mathbf{T}_{w,p}^{n-1}} SE(3)$, since the GU is treated as a point. In contrast, $\mathcal{E}\xi_s^n$ and $\mathcal{E}\xi_p^n$ are their counterparts in the spatial frame, i.e., $\mathcal{E}\xi_s^n, \mathcal{E}\xi_p^n \in se(3)$. In practice, the *control signal* $\mathcal{B}\xi_s^n$, as the body twist, is corrupted by a time-independent additive Gaussian noise [14], $\mathbb{R}^6 \ni \mathcal{B}\xi_w = [\mathcal{B}\nu_w^\top \quad \mathcal{B}\omega_w^\top]^\top \sim \mathcal{N}(\mathbf{0}, \Xi_w)$, with $\Xi_w = \text{diag}(\sigma_{\nu_{\xi,x}}^2, \sigma_{\nu_{\xi,y}}^2, \sigma_{\nu_{\xi,z}}^2, \sigma_{\omega_{\xi,x}}^2, \sigma_{\omega_{\xi,y}}^2, \sigma_{\omega_{\xi,z}}^2) \in \mathbb{R}^{6 \times 6}$. Therefore, the state evolution of relative spatial configurations can be expressed as

$$\mathbf{T}_{s,p}^n = \text{Exp}(-(\mathcal{B}\xi_s^n + \mathcal{B}\xi_w) \Delta t) \cdot \mathbf{T}_{s,p}^{n-1} \cdot \text{Exp}(\mathcal{B}\xi_p^n \Delta t). \quad (5)$$

C. Measurement Model

In the same vein, the measurement model can be interpreted from the perspective of the UAV relative to the GU. Specifically, the reflected signal received at the UAV can be reformulated as follows

$$\mathbf{y}_{s,p}^n = (\mathbf{X}^n \otimes \mathbf{I}_{N_R}) \cdot \mathbf{h}_{s,p}^n + \mathbf{z}_{s,p}^n, \quad (6)$$

$$\mathbf{h}_{s,p}^n = b_{s,p}^n \cdot \omega_{s,p}^n \otimes \mathbf{a}_T(\theta_{s,p}^n, \phi_{s,p}^n) \otimes \mathbf{a}_R(\theta_{s,p}^n, \phi_{s,p}^n), \quad (7)$$

$$\omega_{s,p}^n \triangleq [\omega_{1,s,p}^n, \dots, \omega_{M,s,p}^n]^\top, \quad (8)$$

$$\omega_{m,\nu,s,p}^n = e^{-j2\pi\ell_m f_0 \tau_{s,p}^n} e^{j2\pi\mu_{s,p}^n k_m T_s}, \quad (9)$$

with parameters extracted from $\mathbf{T}_{s,p}^n \triangleq (\mathbf{R}_{s,p}^n, \mathbf{r}_{s,p}^n)$, i.e.,

$$\rho_{s,p}^n = \|\mathbf{r}_{s,p}^n\|, \quad (10)$$

$$\theta_{s,p}^n = \arccos(z_{s,p}^n / \rho_{s,p}^n), \quad (11)$$

$$\phi_{s,p}^n = \text{atan2}(y_{s,p}^n, x_{s,p}^n), \quad (12)$$

$$\tau_{s,p}^n = 2 \cdot \rho_{s,p}^n / c, \quad (13)$$

$$b_{s,p}^n = a \cdot e^{j\varphi_{s,p}^n} / (\rho_{s,p}^n)^2, \quad (14)$$

where $\mathbf{r}_{s,p}^n = [x_{s,p}^n, y_{s,p}^n, z_{s,p}^n]^\top$, scalar c is the speed of light, and the phase shift is assumed to be wide-sense-stationary (WSS), i.e., $\varphi_{s,p}^n = \varphi \sim \mathcal{U}(-\pi, \pi)$. To calculate the Doppler frequency by virtue of the UAV and GU mobility, we first examine their velocities in the global frame $\{w\}$. For the UAV, $\mathbf{s} \in \mathbb{R}^3$ represents the fixed coordinates of the midpoint of the

UPA, relative to the UAV's rotation center, with its representation in *homogeneous coordinates*, i.e., $\bar{\mathbf{s}} = [\mathbf{s}, 1]^\top \in \mathbb{R}^4$. These coordinates are determined by the UPA installation on the UAV platform. The global coordinates are given as ${}^\mathcal{E}\bar{\mathbf{s}}_n = \mathbf{T}_{w,s}^n \bar{\mathbf{s}}$. By taking the time derivative, we obtain its *global velocity* [13], i.e., ${}^\mathcal{E}\bar{\mathbf{v}}_s^n \triangleq \dot{{}^\mathcal{E}\bar{\mathbf{s}}_n} = \dot{\mathbf{T}}_{w,s}^n \bar{\mathbf{s}} = \mathbf{T}_{w,s}^n (\mathcal{B}\boldsymbol{\xi}_s^{n+1})^\wedge \bar{\mathbf{s}} \triangleq \mathbf{T}_{w,s}^n \mathcal{B}\bar{\mathbf{v}}_s^n$, where the property $(\mathcal{B}\boldsymbol{\xi}_s^{n+1})^\wedge = (\mathbf{T}_{w,s}^n)^{-1} \dot{\mathbf{T}}_{w,s}^n$ is utilised [13], and the *local velocity* reads as ${}^\mathcal{B}\bar{\mathbf{v}}_s^n \triangleq (\mathcal{B}\boldsymbol{\xi}_s^{n+1})^\wedge \bar{\mathbf{s}} = [{}^\mathcal{B}\mathbf{v}_s^{n,\top}, 0]^\top$. For the GU, as a single-point target, we consider only the origin of $\{p_n\}$, with its homogeneous coordinates $\bar{\mathbf{p}} = [0, 1]^\top \in \mathbb{R}^4$. Similarly, we have its global velocity ${}^\mathcal{E}\bar{\mathbf{v}}_p^n = \mathbf{T}_{w,p}^n (\mathcal{B}\boldsymbol{\xi}_p^{n+1})^\wedge \bar{\mathbf{p}} = \mathbf{T}_{w,p}^n \mathcal{B}\bar{\mathbf{v}}_p^n$, and the local velocity ${}^\mathcal{B}\bar{\mathbf{v}}_p^n \triangleq (\mathcal{B}\boldsymbol{\xi}_p^{n+1})^\wedge \bar{\mathbf{p}} = [{}^\mathcal{B}\mathbf{v}_p^{n,\top}, 0]^\top$, respectively. Therefore, the *relative velocity vector* in $\{w\}$ is computed as ${}^\mathcal{E}\bar{\mathbf{v}}_{s,p}^n = {}^\mathcal{E}\bar{\mathbf{v}}_p^n - {}^\mathcal{E}\bar{\mathbf{v}}_s^n$. Additionally, the *position vector* is expressed as $\bar{\mathbf{r}}_{s,p}^n = [\mathbf{r}_{s,p}^{n,\top}, 0]^\top \in \mathbb{R}^4$ locally in $\{s_n\}$, with its global representation acquired by pre-multiplying $\mathbf{T}_{w,s}^n$, i.e., ${}^\mathcal{E}\bar{\mathbf{r}}_{s,p}^n = \mathbf{T}_{w,s}^n \bar{\mathbf{r}}_{s,p}^n$. Therefore, the *relative velocity* of $\{p_n\}$ w.r.t. $\{s_n\}$ is given as $v_{\text{radial}}^n = \langle {}^\mathcal{E}\bar{\mathbf{v}}_{s,p}^n, {}^\mathcal{E}\bar{\mathbf{r}}_{s,p}^n \rangle / \rho_{s,p}^n \stackrel{(a)}{=} \langle \mathbf{T}_{s,w}^n {}^\mathcal{E}\bar{\mathbf{v}}_{s,p}^n, \mathbf{T}_{s,w}^n {}^\mathcal{E}\bar{\mathbf{r}}_{s,p}^n \rangle / \rho_{s,p}^n = \langle \mathbf{R}_{s,p}^n \mathcal{B}\mathbf{v}_p^n - \mathcal{B}\mathbf{v}_s^n, \mathbf{r}_{s,p}^n \rangle / \rho_{s,p}^n$, where the property – that a rigid-body motion preserves the inner product of vectors [15] – is applied in (a). Hence, the Doppler frequency is given as

$$\mu_{s,p}^n = 2v_{\text{radial}}^n f_c / c, \quad (15)$$

which indicates that the Doppler frequency is influenced by the control signal $\mathcal{B}\boldsymbol{\xi}_s^{n+1}$. Furthermore, from (11) to (15), the dependence of physical parameters on the relative configuration. Therefore, we express $\zeta_{s,p}^n$ as $\zeta_{s,p}^n(\mathbf{T}_{s,p}^n, \mathcal{B}\boldsymbol{\xi}_s^{n+1})$.

III. THE PROPOSED APPROACH FOR GU TRACKING

A. Extended Kalman Filtering

In this subsection, an Extended Kalman Filtering (EKF) scheme in $SE(3)$ is proposed for GU tracking. The state evolution model is given by (5), where $\mathbf{f}_n : SE(3) \times \mathbb{R}^6 \times \mathbb{R}^6 \rightarrow SE(3)$, while the measurement model by (6), where $\mathbf{g}_n : SE(3) \times \mathbb{R}^6 \rightarrow \mathbb{C}^{MN_R}$, summarised as

$$\begin{aligned} \mathbf{T}_{s,p}^n &= \mathbf{f}_n(\mathbf{T}_{s,p}^{n-1}, \boldsymbol{\xi}_s^n, \boldsymbol{\xi}_w) \oplus \mathbf{w}, \\ \mathbf{y}_{s,p}^n &= \mathbf{g}_n(\mathbf{T}_{s,p}^n, \boldsymbol{\xi}_s^{n+1}) + \mathbf{z}, \end{aligned} \quad (16)$$

where $\boldsymbol{\xi}_s^n$ denotes $\mathcal{B}\boldsymbol{\xi}_s^n$ or $\mathcal{E}\boldsymbol{\xi}_s^n$, and the additive process noise is defined with the *right-plus* operator \oplus , denoted as $\mathbb{R}^6 \ni \mathbf{w} \sim \mathcal{N}(\mathbf{0}, \mathbf{C}_w)$ with $\mathbf{C}_w = \text{diag}(\sigma_{\nu_x}^2, \sigma_{\nu_y}^2, \sigma_{\nu_z}^2, \sigma_{\omega_x}^2, \sigma_{\omega_y}^2, \sigma_{\omega_z}^2) \in \mathbb{R}^{6 \times 6}$. The dependence of $\mathbf{y}_{s,p}^n$ on $\mathbf{T}_{s,p}^n$ is composed as $\mathbf{y}_{s,p}^n = \mathbf{g}_n(\mathbf{h}_{s,p}^n(\zeta_{s,p}^n(\mathbf{T}_{s,p}^n, \cdot)))$.

1) *Prediction step*: The state evolution is linearised around the last a posteriori estimate and control input w.r.t the state variable and process noise, i.e.,

$$\mathbf{F}_{n-1} \triangleq \left. \mathbf{J}_{\mathbf{T}_{s,p}^n}^{\mathbf{T}_{s,p}^n} \right|_{\mathbf{w}=\mathbf{0}} = \mathbf{Ad}_{\text{Exp}(-\mathcal{B}\boldsymbol{\xi}_p^n \Delta t)}, \quad (17)$$

$$\begin{aligned} \mathbf{G}_{n-1} &\triangleq \left. \mathbf{J}_{\mathcal{B}\boldsymbol{\xi}_s^n}^{\mathbf{T}_{s,p}^n} \right|_{\mathbf{T}_{s,p}^n = \hat{\mathbf{T}}_{s,p}^{n-1}, \mathcal{B}\boldsymbol{\xi}_s^n = \mathcal{B}\boldsymbol{\xi}_s^n, \boldsymbol{\xi}_w = \mathbf{0}, \mathbf{w}=\mathbf{0}} \\ &= -\mathbf{Ad}_{\hat{\mathbf{T}}_{s,p}^{n-1}}^{-1} \cdot \mathbf{J}_r(\mathcal{B}\boldsymbol{\xi}_s^n \Delta t) \cdot \Delta t, \end{aligned} \quad (18)$$

$$\mathbf{J}_{\mathbf{T}_{s,p}^{n-1}}^{\mathbf{T}_{s,p}^n} = \mathbf{Ad}_{\text{Exp}(-\mathcal{B}\boldsymbol{\xi}_p^n \Delta t)} \oplus \mathbf{w}, \quad (19)$$

$$\mathbf{J}_{\mathcal{B}\boldsymbol{\xi}_w^n}^{\mathbf{T}_{s,p}^n} = -\mathbf{Ad}_{\mathbf{T}_{s,p}^n}^{-1} \cdot \mathbf{J}_r((\mathcal{B}\boldsymbol{\xi}_s^n + \mathcal{B}\boldsymbol{\xi}_w) \Delta t) \cdot \Delta t. \quad (20)$$

These lead to prediction equations: (i) $\hat{\mathbf{T}}_{s,p}^{n,-} = \mathbf{f}_n(\hat{\mathbf{T}}_{s,p}^{n-1}, \boldsymbol{\xi}_s^n)$. (ii) $\mathbf{P}_n^- = \mathbf{F}_{n-1} \mathbf{P}_{n-1} \mathbf{F}_{n-1}^\top + \mathbf{G}_{n-1} \boldsymbol{\Sigma}_w \mathbf{G}_{n-1}^\top + \mathbf{C}_w$.

Apart from the target tracking, the physical parameters $\zeta_{s,p}^n$ can also be estimated in an intermediate step and subsequently utilized for beamforming design [7]. The conditional distribution of $\mathbf{T}_{s,p}^n$ is characterised as $p(\mathbf{T}_{s,p}^n | \mathbf{y}_{s,p}^{1:n-1}) \sim \mathcal{N}(\hat{\mathbf{T}}_{s,p}^{n,-}, \mathbf{P}_n^-)$. Given the dependence of $\zeta_{s,p}^n$ on $\mathbf{T}_{s,p}^n$, we have the following distribution $p(\zeta_{s,p}^n | \mathbf{y}_{s,p}^{1:n-1}) \sim \mathcal{N}(\hat{\zeta}_{s,p}^{n,-}, \mathbf{V}_n^-)$ with $\hat{\zeta}_{s,p}^{n,-} = \zeta_{s,p}(\hat{\mathbf{T}}_{s,p}^{n,-})$, $\mathbf{V}_n^- = \boldsymbol{\Psi}_n \mathbf{P}_n^- \boldsymbol{\Psi}_n^\top$, and

$$\boldsymbol{\Psi}_n \triangleq \mathbf{J}_{\mathbf{T}_{s,p}^n}^{\zeta_{s,p}^n} \Big|_{\mathbf{T}_{s,p}^n = \hat{\mathbf{T}}_{s,p}^{n,-}, \mathcal{B}\boldsymbol{\xi}_s^{n+1} = \mathcal{B}\boldsymbol{\xi}_s^{n+1}}, \quad (21)$$

where the Jacobian $\mathbf{J}_{\mathbf{T}_{s,p}^n}^{\zeta_{s,p}^n}$ is explained in the sequel.

2) *Correction step*: The measurement model is linearised around the prior estimate w.r.t. the state variable. For brevity, the subscript s, p and superscript n in the sequel are omitted. Considering (6), we obtain $\mathbf{J}_h^y = \mathbf{X} \otimes \mathbf{I}_{N_R} \in \mathbb{C}^{MN_R \times MN_R N_T}$. By leveraging the basic Jacobian blocks [13] in $SE(3)$, the Jacobian \mathbf{J}_ζ^h reads as

$$\begin{aligned} \mathbf{J}_\zeta^h &= [\mathbf{J}_\tau^h \quad \mathbf{J}_\phi^h \quad \mathbf{J}_\theta^h \quad \mathbf{J}_\mu^h] \in \mathbb{C}^{MN_R N_T \times 4} \\ &= (\boldsymbol{\omega} \otimes \mathbf{a}_T^* \otimes \mathbf{a}_R) \bullet \begin{bmatrix} -j2\pi b f_0 \cdot \tilde{\boldsymbol{\ell}}^\top \\ j\pi b \sin \theta \cdot (\mathbf{N}_1 \cdot \mathbf{f}_\phi)^\top \\ j\pi b \cos \theta \cdot (\mathbf{N}_2 \cdot \mathbf{f}_\phi)^\top \\ j2\pi b T_s \cdot \mathbf{k}^\top \end{bmatrix}, \end{aligned} \quad (22)$$

where \bullet indicates the face-splitting product, and components, e.g., \mathbf{k} , \mathbf{N}_1 , depend on the configuration of the OFDM REs.

Proof. Please refer to Appendix V-A. \square

Therefore, the Jacobian \mathbf{J}_ζ^y can be constructed using the chain rule, i.e., $\mathbf{J}_\zeta^y = \mathbf{J}_h^y \cdot \mathbf{J}_\zeta^h \in \mathbb{C}^{MN_R \times 4}$, in the complex domain. In order to enable the correction step in the Lie group, the measurement $\mathbf{y} = \text{Re}\{\mathbf{y}\} + j \cdot \text{Im}\{\mathbf{y}\} \in \mathbb{C}^{MN_R}$ is expressed in its argumented form $\underline{\mathbf{y}} = [\text{Re}\{\mathbf{y}\}^\top \text{Im}\{\mathbf{y}\}^\top]^\top \in \mathbb{R}^{2MN_R}$, with a similar expression for $\underline{\mathbf{z}} \in \mathbb{R}^{2MN_R}$. Thus, the derivative of $\underline{\mathbf{y}}$ w.r.t. ζ reads as $\mathbf{J}_\zeta^{\underline{\mathbf{y}}} = [\text{Re}\{\mathbf{J}_\zeta^y\}^\top \text{Im}\{\mathbf{J}_\zeta^y\}^\top]^\top \in \mathbb{R}^{2MN_R \times 4}$. Furthermore, the structure of $\mathbf{J}_\zeta^{\underline{\mathbf{y}}}$ is summarised as

$$\mathbf{J}_\zeta^{\underline{\mathbf{y}}} = [\mathbf{J}_\tau^{\tau,\top} \quad \mathbf{J}_\tau^{\phi,\top} \quad \mathbf{J}_\tau^{\theta,\top} \quad \mathbf{J}_\tau^{\mu,\top}]^\top, \quad (23)$$

$$\mathbf{J}_\tau^{\tau} = \frac{2}{c\|\mathbf{r}\|} [\mathbf{r}^\top \mathbf{R} \quad \mathbf{0}_{1 \times 3}], \quad (24)$$

$$\mathbf{J}_\tau^{\phi} = \frac{1}{x^2 + y^2} [x \cdot \mathbf{e}_2^\top \mathbf{R} - y \cdot \mathbf{e}_1^\top \mathbf{R} \quad \mathbf{0}_{1 \times 3}], \quad (25)$$

$$\mathbf{J}_\tau^{\theta} = -\frac{1}{\sqrt{\|\mathbf{r}\|^2 - z^2}} [\mathbf{e}_3^\top \mathbf{R} - \frac{z \cdot \mathbf{r}^\top \mathbf{R}}{\|\mathbf{r}\|^2} \quad \mathbf{0}_{1 \times 3}], \quad (26)$$

$$\begin{aligned} \mathbf{J}_\tau^{\mu} &= \frac{2f_c}{c\|\mathbf{r}\|} \left(\left[\mathcal{B}\mathbf{v}_p^\top - \mathcal{B}\mathbf{v}_s^\top \mathbf{R} \quad -\mathbf{r}^\top \mathbf{R} [\mathcal{B}\mathbf{v}_p]_\times \right] \right. \\ &\quad \left. - \|\mathbf{r}\|^{-2} \cdot \langle \mathbf{R} \mathcal{B}\mathbf{v}_p - \mathcal{B}\mathbf{v}_s, \mathbf{r} \rangle \cdot [\mathbf{r}^\top \mathbf{R} \quad \mathbf{0}_{1 \times 3}] \right) \end{aligned} \quad (27)$$

Proof. Please refer to Appendix V-B. \square

By considering the chain rule $\mathbf{J}_{\mathbf{T}}^{\mathbf{y}} = \mathbf{J}_{\zeta}^{\mathbf{y}} \cdot \mathbf{J}_{\mathbf{T}}^{\zeta} \in \mathbb{R}^{2MN_R \times 6}$, the Jacobian $\mathbf{H}_n \in \mathbb{R}^{2MN_R \times 6}$ is obtained as

$$\mathbf{H}_n \triangleq \mathbf{J}_{\mathbf{T}_{s,p}^n}^{\mathbf{y}_{s,p}^n} \Big|_{\mathbf{T}_{s,p}^n = \hat{\mathbf{T}}_{s,p}^{n,-}, \mathcal{B} \xi_s^{n+1} = \mathcal{B} \xi_s^{n+1}}, \quad (28)$$

which leads to correction equations: (i) $\mathbf{S}_n = \mathbf{H}_n \mathbf{P}_n^- \mathbf{H}_n^\top + \mathbf{C}_{\mathbf{z}}$. (ii) $\mathbf{K}_n = \mathbf{P}_n^- \mathbf{H}_n^\top \mathbf{S}_n^{-1}$. (iii) $\hat{\mathbf{T}}_{s,p}^n = \hat{\mathbf{T}}_{s,p}^{n,-} \oplus \mathbf{K}_n (\mathbf{y}_{s,p}^n - \underline{\mathbf{g}}_n(\hat{\mathbf{T}}_{s,p}^{n,-}))$. (iv) $\mathbf{P}_n = \mathbf{P}_n^- - \mathbf{K}_n \mathbf{S}_n \mathbf{K}_n^\top$.

B. Evaluation of the conditional PCRb

The PCRb is defined as the inverse of the Fisher information matrix (FIM) for a random vector-valued parameter [16]. When extended to Lie groups, the recursive structure of the FIM is proven to remain intact [17], given as $\mathcal{I}(X_n) = \mathbf{D}_{n-1}^{22} - \mathbf{D}_{n-1}^{21} (\mathcal{I}(X_{n-1}) + \mathbf{D}_{n-1}^{11})^{-1} \mathbf{D}_{n-1}^{12}$, where $X_n \in \mathcal{G}$ denotes the state variable defined on a Lie group \mathcal{G} , corresponding to $\mathbf{T}_{s,p}^n \in SE(3)$ in our case. See [17] for more details about submatrices, e.g., \mathbf{D}_{n-1}^{11} . For brevity, the following notation is adopted $\mathbf{f}_n(\mathbf{T}_{s,p}^{n-1}) \triangleq \mathbf{f}_n(\mathbf{T}_{s,p}^{n-1}, \xi_s^n, \mathbf{0})$, leading to an approximation via the Baker–Campbell–Hausdorff (BCH) formula [18], i.e., $\mathbf{T}_{s,p}^n \approx \mathbf{f}_n(\mathbf{T}_{s,p}^{n-1}) \text{Exp}(-\text{Ad}_{\mathbf{T}_{s,p}^{n-1}}^{-1} \varepsilon \xi_w \Delta t + \mathbf{w})$. Assuming a concentrated Gaussian distribution [17], the logarithm of the parametrised conditional PDFs are given as $\log p(\mathbf{T}_{s,p}^n | \mathbf{T}_{s,p}^{n-1}) = c_1 + \frac{1}{2} \|\text{Log}(\mathbf{f}_n(\mathbf{T}_{s,p}^{n-1})^{-1} \mathbf{T}_{s,p}^n)\|_{\mathbf{C}_w'}^2$, where $\mathbf{C}_w' \approx \Delta t^2 \cdot \text{Ad}_{\mathbf{T}_{s,p}^{n-1}}^{-1} \Xi_w \text{Ad}_{\mathbf{T}_{s,p}^{n-1}}^{-1, \top} + \mathbf{C}_w$, and c_1 as a constant. Applying the generic expression of \mathbf{D}_{n-1}^{11} leads to $\mathbf{D}_{n-1}^{11} = \mathbf{F}_{n-1}^\top \mathbf{C}_w'^{-1} \mathbf{F}_{n-1}$, where the Jacobian \mathbf{F}_{n-1} is identical to (17). Similarly, we obtain other components $\mathbf{D}_{n-1}^{12} = \mathbf{F}_{n-1}^\top \mathbf{C}_w'^{-1} = \mathbf{D}_{n-1}^{21, \top}$, and $\mathbf{D}_{n-1}^{22} = \mathbf{C}_w'^{-1} + \mathbf{H}_n^\top \mathbf{C}_{\mathbf{z}}^{-1} \mathbf{H}_n$.

By utilising the Woodbury matrix identity [19], we have $\mathcal{I}(\mathbf{T}_{s,p}^n) = \mathbf{H}_n^\top \mathbf{C}_{\mathbf{z}}^{-1} \mathbf{H}_n + (\mathbf{C}_w' + \mathbf{F}_{n-1} \mathcal{I}(\mathbf{T}_{s,p}^{n-1})^{-1} \mathbf{F}_{n-1}^\top)^{-1}$, which has the same form as the conditional PCRb (CPCRb) proposed in [20], i.e., $\mathcal{I}(\mathbf{T}_{s,p}^n | \mathbf{y}_{s,p}^{1:n-1})$, yielding $\text{MSE}(\hat{\mathbf{T}}_{s,p}^n | \mathbf{y}_{s,p}^{1:n-1}) \geq \mathcal{I}(\mathbf{T}_{s,p}^n)^{-1} \triangleq \text{CPCRb}(\mathbf{T}_{s,p}^n)$. Besides, $\text{CPCRb}(\zeta_n)$ can be evaluated via reparameterisation [21], i.e., $\text{CPCRb}(\zeta_{s,p}^n) = \Psi_n \mathcal{I}(\mathbf{T}_{s,p}^n)^{-1} \Psi_n^\top \succ \mathbf{0}$.

IV. PROBLEM FORMULATION FOR CONTROL DESIGN

This work focuses on three tasks: (i) Target tracking, assessed by the estimation of relative spatial configuration $\mathbf{T}_{s,p}^n$. (ii) Physical parameter estimation, relying on the estimation quality of $\mathbf{T}_{s,p}^n$. (iii) Control signal design, which leverages the UAV's mobility to improve tasks (i) and (ii), whose performance can be evaluated via $\text{CPCRb}(\mathbf{T}_{s,p}^n)$ and $\text{CPCRb}(\zeta_{s,p}^n)$, respectively, with optimization criteria [22], e.g., Trace-Opt. Given the dependence of tasks (i) and (ii) on $\mathbf{T}_{s,p}^n$, hereby, control signal design is optimized using Logdet-Opt w.r.t. $\text{CPCRb}(\mathbf{T}_{s,p}^n)$. In the sequel, $\mathbf{T}_n \triangleq \mathbf{T}_{s,p}^n$ for brevity. The optimization problem is formulated as

$$\begin{aligned} \text{P}_1 : \quad & \min_{\xi_s^{n+1}} \log \det(\text{CPCRb}(\mathbf{T}_n)) \\ \text{s.t.} \quad & \|\nu_s^{n+1}\| \leq V_\ell, \quad \|\nu_s^{n+1} - \nu_s^n\| \leq A_\ell, \\ & \|\omega_s^{n+1}\| \leq V_a, \quad \|\omega_s^{n+1} - \omega_s^n\| \leq A_a, \\ & \|\varepsilon \bar{\nu}_s^n - \varepsilon \bar{\nu}_s^{n-1}\| \leq V, \\ & \nu_{s,3}^{n+1} = \omega_{s,1}^{n+1} = \omega_{s,2}^{n+1} = 0, \end{aligned} \quad (29)$$

where V_ℓ represents the maximum allowable linear velocity of the UAV at the n -th epoch, restricting its speed in the horizontal plane. A_ℓ denotes the maximum change in linear velocity between consecutive epochs, limiting acceleration. V_a defines the maximum allowable angular velocity about the UAV's vertical axis at the n -th epoch, while A_a represents the maximum angular velocity change between epochs, limiting angular acceleration. The term V limits the deviation in the global velocity of the midpoint of the UPA implemented on the UAV between consecutive epochs, ensuring smooth trajectory motion, preventing control instability, and enhancing sensing task stability. The last three equality constraints enforce a fixed altitude, prevent tilting, and restrict rotation to the vertical axis. The prior information FIM [23], independent of the control signal, is denoted as $\mathbf{E} \triangleq (\mathbf{C}_w' + \mathbf{F}_{n-1} \mathcal{I}(\mathbf{T}_{n-1})^{-1} \mathbf{F}_{n-1}^\top)^{-1} \succ \mathbf{0}$. Since only Ψ_n in (21) as part of \mathbf{H}_n depends on ξ_s^{n+1} , it can be separated via $\mathbf{A} \triangleq \mathbf{J}_{\zeta}^{\mathbf{y}, \top} \mathbf{J}_{\zeta}^{\mathbf{y}} \succ \mathbf{0}$, enabling the following reformulation

$$\begin{aligned} & \min_{\xi_s^{n+1}} \log \det(\text{CPCRb}(\mathbf{T}_n)) \\ & = \min_{\xi_s^{n+1}} \log \det((\mathbf{E} + \sigma_z^{-2} \Psi_n^\top \mathbf{A} \Psi_n)^{-1}) \\ & = \min_{\xi_s^{n+1}} -\log \det(\tilde{\mathbf{A}}^{-1} + \Psi_n \mathbf{E}^{-1} \Psi_n^\top), \end{aligned} \quad (31)$$

where $\tilde{\mathbf{A}} \triangleq \sigma_z^{-2} \mathbf{A}$. By isolating the component of Ψ_n that depends on ξ_s^{n+1} , problem (P₁) is reformulated as

$$\text{P}_2 : \quad \min_{\xi_s^{n+1}} -\log \det(\tilde{\mathbf{A}}^{-1} + \mathbf{D}_0 + \mathbf{D}) \quad \text{s.t.} \quad (30), \quad (32)$$

with $\mathbf{D} = \mathbf{e}_4 \xi_s^{n+1, \top} \mathbf{K}^\top + \mathbf{K} \xi_s^{n+1} \mathbf{e}_4^\top + \xi_s^{n+1, \top} \tilde{\mathbf{P}} \xi_s^{n+1} \mathbf{e}_4 \mathbf{e}_4^\top$, $\mathbf{K} \triangleq \tilde{\mathbf{E}}^\top \mathbf{M} \mathbf{S}$, $\tilde{\mathbf{P}} \triangleq \mathbf{S}^\top \mathbf{M}^\top \mathbf{E}_{11} \mathbf{M} \mathbf{S} \succ \mathbf{0}$, $\mathbf{S} \triangleq [-[\mathbf{s}]_\times \quad \mathbf{I}]$, where $\tilde{\mathbf{E}} \triangleq [\mathbf{E}_{11} \mathbf{B}^\top \quad \mathbf{E}_{11} \mathbf{c}_{11} + \mathbf{E}_{12} \mathbf{c}_2]$, $\mathbf{M} \triangleq -\frac{2f_c}{c \|\mathbf{r}\|} \cdot \mathbf{R}^\top \mathbf{P}_r^\perp$. The matrices \mathbf{E}_{11} and \mathbf{E}_{12} reads directly from \mathbf{E}^{-1} , while \mathbf{B} , \mathbf{c}_{11} , and \mathbf{c}_2 are the components from Ψ_n .

Proof. Please refer to Appendix VI-A. \square

As \mathbf{D} is convex w.r.t. ξ_s^{n+1} , given that $\tilde{\mathbf{P}} \succ \mathbf{0}$, but the outer $\log \det(\cdot)$ is concave over \mathbb{S}_{++}^4 , the overall function becomes non-convex. Despite \mathbf{D} being a 4×4 matrix, only its last row and column are non-zero, leading to a sparse structure. By leveraging this sparsity, problem (P₂) is reformulated as

$$\text{P}_2' : \quad \max_{\xi_s^{n+1}} \xi_s^{n+1, \top} \tilde{\mathbf{P}} \xi_s^{n+1} + 2\mathbf{c}^\top \xi_s^{n+1}, \quad \text{s.t.} \quad (30). \quad (33)$$

with $\mathbf{c} \triangleq \mathbf{S}^\top \mathbf{M}^\top (\mathbf{E}_{11} \mathbf{c}_{11} + \mathbf{E}_{12} \mathbf{c}_2 - \mathbf{E}_{11} \mathbf{B}^\top \bar{\mathbf{A}}^{-1} \mathbf{a})$, and $\bar{\mathbf{P}} = \mathbf{S}^\top \mathbf{M}^\top \mathbf{E}_{11}^{\frac{1}{2}} (\mathbf{I} - \mathbf{E}_{11}^{\frac{1}{2}} \mathbf{B}^\top \bar{\mathbf{A}}^{-1} \mathbf{B} \mathbf{E}_{11}^{\frac{1}{2}}) \mathbf{E}_{11}^{\frac{1}{2}} \mathbf{M} \mathbf{S}$, where $\bar{\mathbf{A}}$ reads directly from $\bar{\mathbf{A}}^{-1} + \mathbf{D}_0$.

Proof. Please refer to Appendix VI-B. \square

Problem (P'₂) is further expressed in the form of quadratic constrained quadratic programming (QCQP), i.e.,

$$\begin{aligned}
P_3 : \quad & \max_{\xi_s \in \mathbb{R}^6} \xi_s^\top \mathbf{Q}_0 \xi_s + 2\mathbf{c}^\top \xi_s \\
\text{s.t.} \quad & \xi_s^\top \mathbf{Q}_i \xi_s \leq V_i, \quad i = 1, 2, \\
& \xi_s^\top \mathbf{Q}_i \xi_s = 0, \quad i = 4, 5, 6, \\
& \xi_s^\top \mathbf{Q}_i \xi_s - 2\mathbf{b}_i^\top \xi_s + \|\mathbf{b}_i\|^2 \leq A_i, \quad i = 1, 2, \\
& \xi_s^\top \mathbf{Q}_3 \xi_s - 2\mathbf{b}_3^\top \mathbf{R}_2^\top \mathbf{R}_1 \mathbf{S} \xi_s + \|\mathbf{b}_3\|^2 \leq V^2, \\
\text{with} \quad & \mathbf{b}_i = \mathbf{Q}_i \xi_s^n, \quad \mathbf{b}_3 = \mathbf{S} \xi_s^n, \quad i = 1, 2, \\
& \mathbf{R}_2 = \mathbf{R}_{w,s}^{n-1}, \quad \mathbf{R}_1 = \mathbf{R}_{w,s}^n, \\
& \mathbf{Q}_i = \mathbf{e}_i \mathbf{e}_i^\top, \quad i = 4, 5, 6, \\
& \mathbf{Q}_0 = \bar{\mathbf{P}}, \quad \mathbf{Q}_1 = \begin{bmatrix} \mathbf{I}_2 & \\ & \mathbf{0} \end{bmatrix}, \\
& \mathbf{Q}_2 = \mathbf{e}_6 \mathbf{e}_6^\top, \quad \mathbf{Q}_3 = \mathbf{S}^\top \mathbf{S},
\end{aligned} \tag{34}$$

where $V_1 = V_\ell^2$, $V_2 = V_a^2$, $A_1 = A_\ell^2$, $A_2 = A_a^2$, and $\xi_s \triangleq \xi_s^{n+1}$ for brevity. The objective function in (34) is concave, if and only if $\mathbf{I} \preceq \mathbf{E}_{11}^{\frac{1}{2}} \mathbf{B}^\top \bar{\mathbf{A}}^{-1} \mathbf{B} \mathbf{E}_{11}^{\frac{1}{2}}$, requiring all eigenvalues $\lambda_i \geq 1$, which, however, does not always hold true, meaning \mathbf{Q}_0 is solely a symmetric matrix, i.e., $\mathbf{Q}_0 \in \mathbb{S}^6$, and $\mathbf{Q}_i \succcurlyeq \mathbf{0}$, $i = 1, \dots, 6$. Therefore, despite the reduced dimensionality, the problem remains non-convex, akin to (P₂). Problem (P₃) is further homogenized as follows:

$$\begin{aligned}
P'_3 : \quad & \max_{\xi_s \in \mathbb{R}^6, t \in \mathbb{R}} \bar{\xi}_s^\top \bar{\mathbf{Q}}_0 \bar{\xi}_s \\
\text{s.t.} \quad & \bar{\xi}_s^\top \bar{\mathbf{Q}}_i \bar{\xi}_s \leq 1, \quad i = 1, 2, 3, 4, 5, \\
& \bar{\xi}_s^\top \bar{\mathbf{Q}}_i \bar{\xi}_s = 0, \quad i = 6, 7, 8, \\
& \bar{\xi}_s = \begin{bmatrix} \xi_s^\top & t \end{bmatrix}^\top, \quad t^2 = 1. \\
\text{with} \quad & \bar{\mathbf{Q}}_0 = \begin{bmatrix} \mathbf{Q}_0 & \mathbf{c} \\ \mathbf{c}^\top & 0 \end{bmatrix} \in \mathbb{S}^7, \\
& \bar{\mathbf{Q}}_i = \frac{1}{V_i} \cdot \begin{bmatrix} \mathbf{Q}_i & \\ & 0 \end{bmatrix} \succcurlyeq \mathbf{0}, \quad i = 1, 2, \\
& \bar{\mathbf{Q}}_i = \frac{1}{A_{i-2}} \cdot \begin{bmatrix} \mathbf{Q}_{i-2} & -\mathbf{b}_{i-2} \\ -\mathbf{b}_{i-2}^\top & \|\mathbf{b}_{i-2}\|^2 \end{bmatrix} \succcurlyeq \mathbf{0}, \quad i = 3, 4, \\
& \bar{\mathbf{Q}}_5 = \frac{1}{V^2} \cdot \begin{bmatrix} \mathbf{Q}_3 & -\mathbf{S}^\top \mathbf{R}_1^\top \mathbf{R}_2 \mathbf{b}_3 \\ -\mathbf{b}_3^\top \mathbf{R}_2^\top \mathbf{R}_1 \mathbf{S} & \|\mathbf{b}_3\|^2 \end{bmatrix}, \\
& \bar{\mathbf{Q}}_i = \begin{bmatrix} \mathbf{Q}_{i-2} & \\ & 0 \end{bmatrix} \succcurlyeq \mathbf{0}, \quad i = 6, 7, 8,
\end{aligned} \tag{35}$$

where the positive semidefiniteness of $\bar{\mathbf{Q}}_i$, for $i = 3, 4$, is proven via the Theorem 1.20 in [24]: (i) $\mathbf{Q}_{i-2} \succcurlyeq \mathbf{0}$; (ii) $\mathbf{b}_{i-2} \in \mathcal{R}(\mathbf{Q}_{i-2})$; (iii) $\|\mathbf{b}_{i-2}\|^2 - \mathbf{b}_{i-2}^\top \mathbf{Q}_{i-2} \mathbf{b}_{i-2} = 0$, thus, $\bar{\mathbf{Q}}_i / \mathbf{Q}_{i-2} \succcurlyeq \mathbf{0}$. The same applied to $\bar{\mathbf{Q}}_5$, assuming

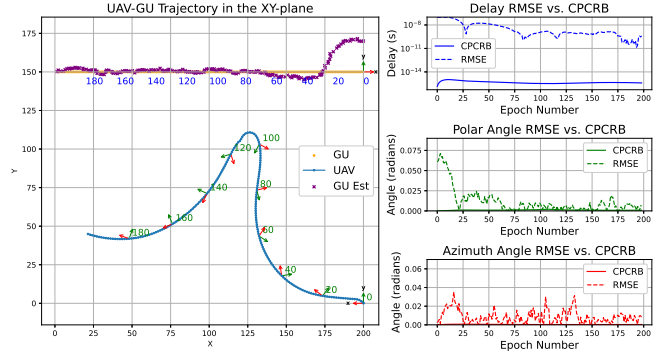


Fig. 1. the UAV trajectory, RMSE vs. CPRB Metrics for optimised setting.

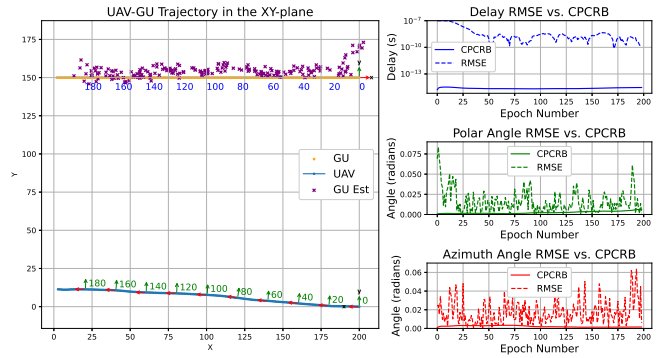


Fig. 2. the UAV trajectory, RMSE vs. CPRB Metrics for parallel setting.

$\mathbf{R}_1 \approx \mathbf{R}_2$. The semidefinite relaxation (SDR) is applied and solved using convex solvers, e.g., CVX. Subsequently, a rank-one approximation is extracted using Gaussian randomization. If random samples are infeasible, a rescaling step ensures feasibility.

Remark 1. The objective function resembles a local cost-to-go function for an elementary transition in the context of MPC, which seeks to minimize the total cost over a finite horizon. However, directly applying this analogy presents several challenges: (i) There is no well-defined reference for using control ξ^* to maintain the equilibrium state \mathbf{T}^* ; (ii) The objective function exhibits a highly nonlinear dependence on the state through \mathbf{c} and $\bar{\mathbf{P}}$, rather than being merely the distance to the reference with some chosen metrics. (iii) This local approach may not align well with the global optimal trajectory over the long term.

A. Numerical Results

In this section, we analyze the performance of target tracking and the trajectory generation via control signal design. Key simulation parameters are as follows: $N_T = N_R = 2 \times 2 = 4$, $f_c = 2.4$ GHz, $L = 32$, $K = 10$, $\sigma_{RCS} = 0.5$ m, $\mathbf{s} = [0.2, 0.3, 0.1]^\top$ m, $\Delta t = 0.25$ s, $N = 200$, $V_\ell = 6$ m/s, $V_a = 0.15$ rad/s, $A_\ell = 2$ m/s, $A_a = 0.05$ rad/s, $V = 0.5$ m/s, $L_\xi = 200$. The initial GU configuration is

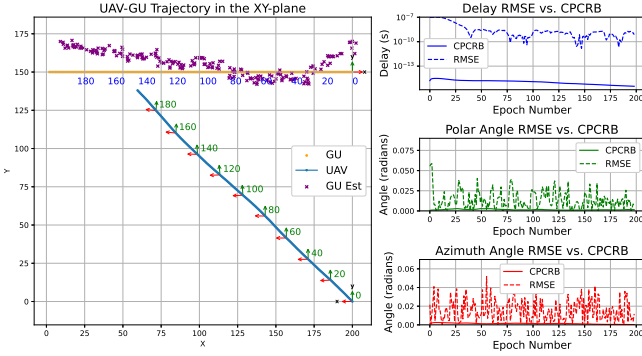


Fig. 3. the UAV trajectory, RMSE vs. CPCRB Metrics for diagonal setting.

set as $\mathbf{T}_{w,p}^0 = (\mathbf{I}_3, [200, 150, 0]^\top \text{m})$, i.e., its axes align with the world frame. The GU moves with constant velocity 4m/s, along the x-axis from right to left. The UAV begins at $\mathbf{T}_{w,s}^0 = (\text{diag}(-1, 1, -1), [200, 0, 150]^\top \text{m})$, i.e., with its axes rotated 180° about the y-axis, with the initial control $\mathbf{B}\boldsymbol{\xi}_s^0 = [0, 1, \mathbf{0}_4^\top]^\top$. The EKF is initialized using a coarse estimate of the GU position $\hat{\mathbf{r}}_{w,p}^0 = [200, 170, 0]^\top \text{m}$. We evaluate radar sensing performance in terms of root mean square error (RMSE) for delay, polar, and azimuthal angles—key metrics in radar applications—by comparing three UAV trajectory designs: (i) an optimized trajectory obtained by control signal design (Fig. 1), (ii) a parallel trajectory (Fig. 2), where the UAV’s motion aligns with the GU’s, and (iii) a diagonal trajectory (Fig. 3), where the UAV approaches the GU at a 45° -angle with the identical velocity as in (ii).

First, we examine the UAV trajectory in the XY-plane w.r.t. different trajectories: The optimized trajectory achieves better convergence of the GU position estimates. In the parallel setting, the UAV’s motion deviates slightly from the GU’s path due to control noise $\boldsymbol{\xi}_w$, and the GU position estimates show acceptable accuracy but low precision. In the diagonal trajectory, as the UAV approaches the GU, the location estimates exhibit significant systematic deviations from the true values, i.e., with high precision but low accuracy. This might be attributed to the increasing relative velocity between the UAV and the GU, which could limit the EKF’s ability to adapt quickly to rapid changes. A similar phenomenon is observed in [7], where RMSE spikes occur, despite a decreasing PCRb, as the vehicle passes in front of the radar. Secondly, we evaluate the RMSE vs. CPCRB metrics among these trajectories. The optimized trajectory outperforms the heuristic designs, with RMSE decreasing steadily and stabilizing close to the CRLB (RMSE of polar and azimuth angles stays below 0.02 rad), despite: (i) a stabilizing stage in terms of delay estimate between 25-75 epochs; (ii) it requiring more epochs (>25) to converge to the true parameter values compared to the heuristic designs. In contrast, the parallel and diagonal trajectories converge faster but have little tendency to maintain accuracy or precision.

B. Conclusion

This paper develops a novel UAV-enabled MIMO-OFDM ISAC system that incorporates UPA configurations and rigid-body dynamics via $SE(3)$, enabling both target tracking and trajectory design from a control perspective. It highlights that the performance of target tracking and parameter estimation depends not only on the geometric relationship between the UAV and the GU but also on the dynamic changes within the system, underscoring the critical role of UAV trajectory design in enhancing radar sensing performance.

V. APPENDIX A

A. Computation of Jacobian block \mathbf{J}_ζ^h

The dependence of the transmit and receive array response vectors on polar and azimuthal angles is omitted for simplicity, i.e., $\mathbf{a}_T \triangleq \mathbf{a}_T(\theta, \phi)$, $\mathbf{a}_R \triangleq \mathbf{a}_R(\theta, \phi)$.

a) \mathbf{j}_τ^h : Considering (13) and (14), there exist an invertible function between $\tau \in \mathbb{R}_+$ and $|b| \in \mathbb{R}_+$, allowing $|b|$ to be fully expressed in terms of τ . Therefore,

$$\begin{aligned} \mathbf{j}_\tau^h &= b' \cdot \boldsymbol{\omega} \otimes \mathbf{a}_T^* \otimes \mathbf{a}_R + b \cdot \mathbf{j}_\tau^w \otimes \mathbf{a}_T^* \otimes \mathbf{a}_R \\ &= -\frac{2b}{\tau} (\boldsymbol{\omega} \otimes \mathbf{a}_T^* \otimes \mathbf{a}_R) - j2\pi b f_0 \cdot (\boldsymbol{\omega} \otimes \mathbf{a}_T^* \otimes \mathbf{a}_R) \odot \boldsymbol{\ell} \\ &\triangleq -j2\pi b f_0 \cdot (\boldsymbol{\omega} \otimes \mathbf{a}_T^* \otimes \mathbf{a}_R) \odot \tilde{\boldsymbol{\ell}}, \end{aligned} \quad (36)$$

where $\mathbb{R}^{MN_T N_R} \ni \boldsymbol{\ell} \triangleq \boldsymbol{\ell}_0 \otimes \mathbf{1}_{N_T N_R}$ is a constant and deterministic vector with $\boldsymbol{\ell}_0 \triangleq [\ell_1, \dots, \ell_M]^\top$ which only depends on the RE and UPA configuration, operator \odot is the Hadamard product and the property $(\mathbf{A} \odot \mathbf{C}) \otimes (\mathbf{B} \odot \mathbf{D}) = (\mathbf{A} \otimes \mathbf{B}) \odot (\mathbf{C} \otimes \mathbf{D})$ is applied, assuming \mathbf{A} has the same dimensions of \mathbf{C} and \mathbf{B} with \mathbf{D} , thus, $(\mathbf{a} \odot \mathbf{c}) \otimes \mathbf{b} = (\mathbf{a} \otimes \mathbf{b}) \odot (\mathbf{c} \otimes \mathbf{1})$.

b) \mathbf{j}_μ^h : Following the same procedure in (36), we give the resultant Jacobian directly, i.e.,

$$\mathbf{j}_\mu^h = j2\pi b T_s \cdot (\boldsymbol{\omega} \otimes \mathbf{a}_T^* \otimes \mathbf{a}_R) \odot \mathbf{k}, \quad (37)$$

where $\mathbb{R}^{MN_T N_R} \ni \mathbf{k} \triangleq \mathbf{k}_0 \otimes \mathbf{1}_{N_T N_R}$ is a constant and deterministic vector with $\mathbf{k}_0 \triangleq [k_1, \dots, k_M]^\top$ which only depends on the RE and UPA configuration,

c) \mathbf{j}_ϕ^h : Hereby, we give its derivation as follows

$$\mathbf{j}_\phi^h = b \cdot \boldsymbol{\omega} \otimes \left[\mathbf{j}_\phi^{\mathbf{a}_{T,y}^*} \otimes \mathbf{a}_{T,x}^* \otimes \mathbf{a}_{R,y} \otimes \mathbf{a}_{R,x} \right. \quad (38)$$

$$\left. + \mathbf{a}_{T,y}^* \otimes \mathbf{j}_\phi^{\mathbf{a}_{T,x}^*} \otimes \mathbf{a}_{R,y} \otimes \mathbf{a}_{R,x} \right] \quad (39)$$

$$\left. + \mathbf{a}_{T,y}^* \otimes \mathbf{a}_{T,x}^* \otimes \mathbf{j}_\phi^{\mathbf{a}_{R,y}} \otimes \mathbf{a}_{R,x} \right] \quad (40)$$

$$\left. + \mathbf{a}_{T,y}^* \otimes \mathbf{a}_{T,x}^* \otimes \mathbf{a}_{R,y} \otimes \mathbf{j}_\phi^{\mathbf{a}_{R,x}} \right], \quad (41)$$

in the following, the computation for the first term in the brackets is provided and the remaining terms can be derived straightforwardly and directly given.

$$\begin{aligned} (38): \quad & \mathbf{j}_\phi^{\mathbf{a}_{T,y}^*} \otimes \mathbf{a}_{T,x}^* \otimes \mathbf{a}_{R,y} \otimes \mathbf{a}_{R,x} \\ &= j\pi \sin \theta \cos \phi \cdot (\mathbf{a}_{T,y}^* \odot \mathbf{n}_{T,y}) \otimes \mathbf{a}_{T,x}^* \otimes \mathbf{a}_{R,y} \otimes \mathbf{a}_{R,x} \\ &= j\pi \sin \theta \cos \phi \cdot (\mathbf{a}_T^* \otimes \mathbf{a}_R) \odot (\mathbf{n}_{T,y} \otimes \mathbf{1} \otimes \mathbf{1} \otimes \mathbf{1}), \end{aligned}$$

The other three terms are given as

$$(39): \quad -j\pi \sin \theta \sin \phi \cdot (\mathbf{a}_T^* \otimes \mathbf{a}_R) \odot (\mathbf{1} \otimes \mathbf{n}_{T,x} \otimes \mathbf{1} \otimes \mathbf{1}),$$

$$(40): \quad -j\pi \sin \theta \cos \phi \cdot (\mathbf{a}_T^* \otimes \mathbf{a}_R) \odot (\mathbf{1} \otimes \mathbf{1} \otimes \mathbf{n}_{R,y} \otimes \mathbf{1}),$$

$$(41): \quad j\pi \sin \theta \sin \phi \cdot (\mathbf{a}_T^* \otimes \mathbf{a}_R) \odot (\mathbf{1} \otimes \mathbf{1} \otimes \mathbf{1} \otimes \mathbf{n}_{R,x}),$$

$$\mathbf{n}_{T,x} \triangleq \frac{1}{\sqrt{N_{T,x}}} [0, \dots, N_{T,x} - 1]^\top, \mathbf{n}_{T,y} \triangleq \frac{1}{\sqrt{N_{T,y}}} [0, \dots, N_{T,y} - 1]^\top,$$

$$\mathbf{n}_{R,x} \triangleq \frac{1}{\sqrt{N_{R,x}}} [0, \dots, N_{R,x} - 1]^\top, \mathbf{n}_{R,y} \triangleq \frac{1}{\sqrt{N_{R,y}}} [0, \dots, N_{R,y} - 1]^\top.$$

Therefore, we have

$$\mathbf{j}_\phi^h = j\pi b \sin \theta \cdot \boldsymbol{\omega} \otimes \left[(\mathbf{a}_T^* \otimes \mathbf{a}_R) \odot \left(\cos \phi (\mathbf{n}_{T,y} \otimes \mathbf{1} \otimes \mathbf{1} \otimes \mathbf{1}) - \sin \phi (\mathbf{1} \otimes \mathbf{n}_{T,x} \otimes \mathbf{1} \otimes \mathbf{1}) - \cos \phi (\mathbf{1} \otimes \mathbf{1} \otimes \mathbf{n}_{R,y} \otimes \mathbf{1}) + \sin \phi (\mathbf{1} \otimes \mathbf{1} \otimes \mathbf{1} \otimes \mathbf{n}_{R,x}) \right) \right]$$

$$= j\pi b \sin \theta \cdot \boldsymbol{\omega} \otimes (\mathbf{a}_T^* \otimes \mathbf{a}_R) \odot \left[\cos \phi (\mathbf{1} \otimes \mathbf{n}_{T,y} \otimes \mathbf{1} \otimes \mathbf{1} \otimes \mathbf{1}) - \sin \phi (\mathbf{1} \otimes \mathbf{1} \otimes \mathbf{n}_{T,x} \otimes \mathbf{1} \otimes \mathbf{1}) - \cos \phi (\mathbf{1} \otimes \mathbf{1} \otimes \mathbf{1} \otimes \mathbf{n}_{R,y} \otimes \mathbf{1}) + \sin \phi (\mathbf{1} \otimes \mathbf{1} \otimes \mathbf{1} \otimes \mathbf{1} \otimes \mathbf{n}_{R,x}) \right]$$

$$= j\pi b \sin \theta \cdot (\boldsymbol{\omega} \otimes \mathbf{a}_T^* \otimes \mathbf{a}_R) \odot (\mathbf{N}_1 \cdot \mathbf{f}_\phi), \quad (42)$$

where the property $\mathbf{a} \otimes (\mathbf{b} \odot \mathbf{d}) = (\mathbf{a} \otimes \mathbf{b}) \odot (\mathbf{1} \otimes \mathbf{d})$ is applied, with $\mathbf{N}_1 \in \mathbb{R}^{MN_T N_R \times 4}$ as a constant and deterministic matrix, which only depends on the RE and UPA configuration, i.e.,

$$\mathbf{N}_1 \triangleq \begin{bmatrix} (\mathbf{1}_M \otimes \mathbf{n}_{T,y} \otimes \mathbf{1}_{N_{T,x}} \otimes \mathbf{1}_{N_{R,y}} \otimes \mathbf{1}_{N_{R,x}})^\top \\ (\mathbf{1}_M \otimes \mathbf{1}_{N_{T,y}} \otimes \mathbf{n}_{T,x} \otimes \mathbf{1}_{N_{R,y}} \otimes \mathbf{1}_{N_{R,x}})^\top \\ (\mathbf{1}_M \otimes \mathbf{1}_{N_{T,y}} \otimes \mathbf{1}_{N_{T,x}} \otimes \mathbf{n}_{R,y} \otimes \mathbf{1}_{N_{R,x}})^\top \\ (\mathbf{1}_M \otimes \mathbf{1}_{N_{T,y}} \otimes \mathbf{1}_{N_{T,x}} \otimes \mathbf{1}_{N_{R,y}} \otimes \mathbf{n}_{R,x})^\top \end{bmatrix}^\top, \quad (43)$$

where the dimension of each vector $\mathbf{1}$ is specified across (38)-(42), and the \mathbf{f}_ϕ as a function of polar angle is given as $\mathbf{f}_\phi = [\cos \phi \quad -\sin \phi \quad -\cos \phi \quad \sin \phi]^\top$.

d) \mathbf{j}_θ^h : Following the similar process from (38)-(42), we obtain

$$\mathbf{j}_\theta^h = j\pi b \cos \theta \cdot \boldsymbol{\omega} \otimes (\mathbf{a}_T^* \otimes \mathbf{a}_R) \odot \left[\sin \phi (\mathbf{1} \otimes \mathbf{n}_{T,y} \otimes \mathbf{1} \otimes \mathbf{1} \otimes \mathbf{1}) + \cos \phi (\mathbf{1} \otimes \mathbf{1} \otimes \mathbf{n}_{T,x} \otimes \mathbf{1} \otimes \mathbf{1}) - \sin \phi (\mathbf{1} \otimes \mathbf{1} \otimes \mathbf{1} \otimes \mathbf{n}_{R,y} \otimes \mathbf{1}) - \cos \phi (\mathbf{1} \otimes \mathbf{1} \otimes \mathbf{1} \otimes \mathbf{1} \otimes \mathbf{n}_{R,x}) \right]$$

$$= j\pi b \cos \theta \cdot (\boldsymbol{\omega} \otimes \mathbf{a}_T^* \otimes \mathbf{a}_R) \odot (\mathbf{N}_2 \cdot \mathbf{f}_\phi), \quad (44)$$

with $\mathbf{N}_2 \in \mathbb{R}^{MN_T N_R \times 4}$ as another constant and deterministic matrix, which can be derived from \mathbf{N}_1 , i.e.,

$$\mathbf{N}_2 \triangleq \mathbf{N}_1 \cdot \begin{bmatrix} 0 & -1 & 0 & 0 \\ 0 & 0 & -1 & 0 \\ 0 & 0 & 0 & -1 \\ 1 & 0 & 0 & 0 \end{bmatrix}. \quad (45)$$

B. Computation of Jacobian block \mathbf{J}_T^ζ

a) \mathbf{J}_T^τ : Considering (13), the dependence of delay τ on \mathbf{T} is explicitly denoted as

$$\tau = \frac{2}{c} \|\mathbf{r}\| = \frac{2}{c} \|g_{\mathbf{T}}(\mathbf{0})\|. \quad (46)$$

Therefore, we have

$$\mathbf{J}_T^\tau = \frac{\partial \tau}{\partial \mathbf{T}} = \frac{2}{c} \frac{\partial \|\mathbf{r}\|}{\partial \mathbf{r}} \frac{\partial \mathbf{r}}{\partial \mathbf{T}} = \frac{2}{c} \frac{\mathbf{r}^\top}{\|\mathbf{r}\|} \mathbf{J}_T^{g_{\mathbf{T}}(\mathbf{0})}$$

$$= \frac{2}{c} \frac{\mathbf{r}^\top}{\|\mathbf{r}\|} [\mathbf{R} \quad -\mathbf{R}[\mathbf{0}]_\times] = \frac{2}{c} \frac{\mathbf{r}^\top}{\|\mathbf{r}\|} [\mathbf{R} \quad \mathbf{0}_{3 \times 3}]. \quad (47)$$

b) \mathbf{J}_T^μ : Considering (15) and (??), the dependence of delay μ on \mathbf{T} is explicitly denoted as

$$\mu = \frac{2f_c}{c\|\mathbf{r}\|} \langle \mathbf{T}^{\mathcal{B}} \bar{\mathbf{v}}_p - \mathcal{B} \bar{\mathbf{v}}_s, \bar{\mathbf{r}} \rangle = \frac{2f_c}{c\|\mathbf{r}\|} \langle \mathbf{R}^{\mathcal{B}} \mathbf{v}_p - \mathcal{B} \mathbf{v}_s, \mathbf{r} \rangle$$

$$= \frac{2f_c}{c\|\mathbf{r}\|} (\langle g_{\mathbf{T}^*}(\mathcal{B} \bar{\mathbf{v}}_p) - \mathcal{B} \bar{\mathbf{v}}_s, g_{\mathbf{T}}(\bar{\mathbf{0}}) - \bar{\mathbf{0}} \rangle)$$

$$= \frac{2f_c}{c\|\mathbf{r}\|} (\langle g_{\mathbf{T}^*}(\mathcal{B} \bar{\mathbf{v}}_p) - \mathcal{B} \bar{\mathbf{v}}_s, g_{\mathbf{T}}(\bar{\mathbf{0}}) \rangle)$$

$$= \frac{2f_c}{c\|\mathbf{r}\|} (\langle g_{\mathbf{T}^*}(\mathcal{B} \bar{\mathbf{v}}_p), g_{\mathbf{T}}(\bar{\mathbf{0}}) \rangle - \langle \mathcal{B} \mathbf{v}_s, g_{\mathbf{T}}(\bar{\mathbf{0}}) \rangle). \quad (48)$$

The intermediate Jacobian blocks are obtained as follows

$$\frac{\partial \|\mathbf{r}\|^{-1}}{\partial \mathbf{T}} = \frac{\partial \|\mathbf{r}\|^{-1}}{\partial \mathbf{r}} \frac{\partial \mathbf{r}}{\partial \mathbf{T}} = -\|\mathbf{r}\|^{-3} \cdot \mathbf{r}^\top [\mathbf{R} \quad \mathbf{0}_{3 \times 3}], \quad (49)$$

$$\frac{\partial}{\partial \mathbf{T}} \langle \mathcal{B} \mathbf{v}_s, g_{\mathbf{T}}(\bar{\mathbf{0}}) \rangle = \mathcal{B} \mathbf{v}_s^\top \mathbf{J}_T^{g_{\mathbf{T}}(\bar{\mathbf{0}})} = \mathcal{B} \mathbf{v}_s^\top [\mathbf{R} \quad \mathbf{0}_{3 \times 3}], \quad (50)$$

$$\frac{\partial}{\partial \mathbf{T}} \langle g_{\mathbf{T}^*}(\mathcal{B} \bar{\mathbf{v}}_p), g_{\mathbf{T}}(\bar{\mathbf{0}}) \rangle = [\mathcal{B} \mathbf{v}_p^\top \quad -\mathbf{r}^\top \mathbf{R} [\mathcal{B} \mathbf{v}_p]_\times], \quad (51)$$

The proof of (51) is given in the sequel. Thus, we have

$$\mathbf{J}_T^\mu = \frac{2f_c}{c\|\mathbf{r}\|} \left([\mathcal{B} \mathbf{v}_p^\top - \mathcal{B} \mathbf{v}_s^\top \mathbf{R} \quad -\mathbf{r}^\top \mathbf{R} [\mathcal{B} \mathbf{v}_p]_\times] \right. \\ \left. - \|\mathbf{r}\|^{-2} \cdot \langle \mathbf{R}^{\mathcal{B}} \mathbf{v}_p - \mathcal{B} \mathbf{v}_s, \mathbf{r} \rangle \cdot [\mathbf{r}^\top \mathbf{R} \quad \mathbf{0}_{1 \times 3}] \right). \quad (52)$$

Proof. Let $f: SE(3) \rightarrow \mathbb{R}$, $\mathbf{T} \mapsto f(\mathbf{T}) = \langle g_{\mathbf{T}^*}(\bar{\mathbf{v}}), g_{\mathbf{T}}(\bar{\mathbf{0}}) \rangle$, where $g_{\mathbf{T}}(\cdot)$ denotes the homogeneous representations of the motion actions, which share the same expression on points and vectors, i.e., $g_{\mathbf{T}^*}(\bar{\mathbf{v}}) = g_{\mathbf{T}}(\bar{\mathbf{v}})$. While $\bar{\mathbf{v}}$ are the homogeneous coordinates of a vector $\mathbf{v} \in \mathbb{R}^3$, i.e., $\bar{\mathbf{v}} = [\mathbf{v}^\top, 0]^\top \in \mathbb{R}^4$, $\bar{\mathbf{0}}$ is the homogeneous representation of the origin $\mathbf{0} \in \mathbb{R}^3$, i.e., $\mathbf{e}_4 = \bar{\mathbf{0}} = [\mathbf{0}^\top, 1]^\top \in \mathbb{R}^4$. Taking the directional derivative of $f(\mathbf{T})$ along the direction $\boldsymbol{\tau} = [\boldsymbol{\rho}^\top, \boldsymbol{\theta}^\top]^\top$ in the local tangent space, we have

$$\mathbf{D}_\tau f(\mathbf{T}) = \lim_{t \rightarrow 0} \frac{\langle (\mathbf{T} \oplus t\boldsymbol{\tau}) \bar{\mathbf{v}}, (\mathbf{T} \oplus t\boldsymbol{\tau}) \mathbf{e}_4 \rangle - \langle \mathbf{T} \bar{\mathbf{v}}, \mathbf{T} \mathbf{e}_4 \rangle}{t}$$

$$= \lim_{t \rightarrow 0} \frac{\langle \mathbf{T} \cdot \text{Exp}(t\boldsymbol{\tau}) \cdot \bar{\mathbf{v}}, \mathbf{T} \cdot \text{Exp}(t\boldsymbol{\tau}) \cdot \mathbf{e}_4 \rangle - \langle \mathbf{T} \bar{\mathbf{v}}, \mathbf{T} \mathbf{e}_4 \rangle}{t}$$

$$\approx \lim_{t \rightarrow 0} \frac{\langle \mathbf{R}(\mathbf{I} + t[\boldsymbol{\theta}]_\times) \mathbf{v}, t\mathbf{R}\boldsymbol{\rho} + \mathbf{r} \rangle - \langle \mathbf{R}\mathbf{v}, \mathbf{r} \rangle}{t}$$

$$= \lim_{t \rightarrow 0} \frac{\langle \mathbf{R}\mathbf{v}, t\mathbf{R}\boldsymbol{\rho} \rangle + \langle t\mathbf{R}[\boldsymbol{\theta}]_\times \mathbf{v}, t\mathbf{R}\boldsymbol{\rho} \rangle + \langle t\mathbf{R}[\boldsymbol{\theta}]_\times \mathbf{v}, \mathbf{r} \rangle}{t}$$

$$= \mathbf{v}^\top \boldsymbol{\rho} + \mathbf{r}^\top \mathbf{R}[\boldsymbol{\theta}]_\times \mathbf{v} = [\mathbf{v}^\top \quad -\mathbf{r}^\top \mathbf{R}[\boldsymbol{\theta}]_\times] \cdot \boldsymbol{\tau}, \quad (53)$$

where we applied the property $[\mathbf{a}]_\times \mathbf{b} = -[\mathbf{b}]_\times \mathbf{a}$ and the approximation given as

$$\text{Exp}(t\boldsymbol{\tau}) \approx \begin{bmatrix} \mathbf{I} + t[\boldsymbol{\theta}]_\times & t\boldsymbol{\rho} \\ \mathbf{0} & 1 \end{bmatrix}. \quad (54)$$

Therefore, for the given $f(\mathbf{T})$, the differential map $Df(\mathbf{T})$ has a matrix form and the associated composition corresponds to the matrix-vector multiplication, i.e., $Df(\mathbf{T}) = \frac{\partial f(\mathbf{T})}{\partial \mathbf{T}} = [\mathbf{v}^\top \quad -\mathbf{r}^\top \mathbf{R} [\mathbf{v}]_\times]$. \square

c) $\mathbf{J}_{\mathbf{T}}^\theta$: Considering (11), the dependence of delay θ on \mathbf{T} is explicitly denoted as

$$\begin{aligned} \theta &= \text{accos} \left(\frac{z}{\|\mathbf{r}\|} \right) = \text{accos} \left(\frac{\langle \mathbf{e}_3, \mathbf{r} \rangle}{\|\mathbf{r}\|} \right) \\ &= \text{accos} \left(\frac{\langle \mathbf{e}_3, g_{\mathbf{T}}(\mathbf{0}) \rangle}{\|\mathbf{r}\|} \right), \end{aligned} \quad (55)$$

where $\mathbf{e}_3 = [0, 0, 1]^\top \in \mathbb{R}^3$ is used to extract the element z from \mathbf{r} . We have the following Jacobian block

$$\begin{aligned} \frac{\partial}{\partial \mathbf{T}} \frac{\langle \mathbf{e}_3, g_{\mathbf{T}}(\mathbf{0}) \rangle}{\|\mathbf{r}\|} &= \frac{1}{\|\mathbf{r}\|} \frac{\partial}{\partial \mathbf{T}} \langle \mathbf{e}_3, g_{\mathbf{T}}(\mathbf{0}) \rangle + z \cdot \frac{\partial \|\mathbf{r}\|^{-1}}{\partial \mathbf{T}} \\ &= \frac{1}{\|\mathbf{r}\|} \left([\mathbf{e}_3^\top \mathbf{R} \quad \mathbf{0}_{1 \times 3}] - \frac{z}{\|\mathbf{r}\|^2} \cdot [\mathbf{r}^\top \mathbf{R} \quad \mathbf{0}_{1 \times 3}] \right). \end{aligned} \quad (56)$$

Therefore, we have

$$\begin{aligned} \mathbf{J}_{\mathbf{T}}^\theta &= -\frac{1}{\sqrt{1 - (z/\|\mathbf{r}\|)^2}} \cdot \frac{\partial}{\partial \mathbf{T}} \frac{\langle \mathbf{e}_3, g_{\mathbf{T}}(\mathbf{0}) \rangle}{\|\mathbf{r}\|} \\ &= -\frac{1}{\sqrt{\|\mathbf{r}\|^2 - z^2}} \left[\mathbf{e}_3^\top \mathbf{R} - \frac{z \mathbf{r}^\top \mathbf{R}}{\|\mathbf{r}\|^2} \quad \mathbf{0}_{1 \times 3} \right]. \end{aligned} \quad (57)$$

d) $\mathbf{J}_{\mathbf{T}}^\phi$: Considering (12), the dependence of delay ϕ on \mathbf{T} is explicitly denoted as

$$\begin{aligned} \phi &= \text{atan2}(y, x) = \text{atan2}(\langle \mathbf{e}_2, \mathbf{r} \rangle, \langle \mathbf{e}_1, \mathbf{r} \rangle) \\ &= \text{atan2}(\langle \mathbf{e}_2, g_{\mathbf{T}}(\mathbf{0}) \rangle, \langle \mathbf{e}_1, g_{\mathbf{T}}(\mathbf{0}) \rangle), \end{aligned} \quad (58)$$

where $\mathbf{e}_2 = [0, 1, 0]^\top \in \mathbb{R}^3$ and $\mathbf{e}_1 = [1, 0, 0]^\top \in \mathbb{R}^3$ are used to extract the element y and x from \mathbf{r} , respectively. Therefore, we have

$$\begin{aligned} \mathbf{J}_{\mathbf{T}}^\phi &= \frac{\partial \phi}{\partial x} \cdot \frac{\partial x}{\partial \mathbf{T}} + \frac{\partial \phi}{\partial y} \cdot \frac{\partial y}{\partial \mathbf{T}} \\ &= \frac{-y}{x^2 + y^2} [\mathbf{e}_1^\top \mathbf{R} \quad \mathbf{0}_{1 \times 3}] + \frac{x}{x^2 + y^2} [\mathbf{e}_2^\top \mathbf{R} \quad \mathbf{0}_{1 \times 3}] \\ &= \frac{1}{x^2 + y^2} [x \cdot \mathbf{e}_2^\top \mathbf{R} - y \cdot \mathbf{e}_1^\top \mathbf{R} \quad \mathbf{0}_{1 \times 3}]. \end{aligned} \quad (59)$$

VI. APPENDIX B

A. Trajectory Optimization Formulation as (P₂)

The subscript n is omitted in the following for simplicity. According to (21) and (23), $\Psi \in \mathbb{R}^{4 \times 6}$ can be partitioned into

$$\Psi = \begin{bmatrix} \mathbf{B} & \mathbf{0} \\ \mathbf{c}_1^\top & \mathbf{c}_2^\top \end{bmatrix} = \begin{bmatrix} \mathbf{B} & \mathbf{0} \\ \mathbf{c}_{11}^\top & \mathbf{c}_2^\top \end{bmatrix} + \begin{bmatrix} \mathbf{0} & \mathbf{0} \\ \mathbf{c}_{12}^\top & \mathbf{0} \end{bmatrix} \triangleq \Psi_1 + \Psi_2, \quad (60)$$

with

$$\mathbf{c}_{11}^\top = \frac{2f_c}{c\|\mathbf{r}\|} \cdot {}^B \mathbf{v}_p^\top \mathbf{R}^\top \mathbf{P}_r^\perp \mathbf{R}, \quad (61)$$

$$\mathbf{c}_{12}^\top = -\frac{2f_c}{c\|\mathbf{r}\|} \cdot {}^B \mathbf{v}_s^\top \mathbf{P}_r^\perp \mathbf{R}, \quad (62)$$

$$\mathbf{c}_2^\top = -\frac{2f_c}{c\|\mathbf{r}\|} \cdot \mathbf{r}^\top \mathbf{R} [{}^B \mathbf{v}_p]_\times, \quad (63)$$

and $\mathbf{B} \in \mathbb{R}^{3 \times 3}$ is the remaining non-zero block. $\mathbf{P}_r^\perp \triangleq \mathbf{I} - \mathbf{r} \mathbf{r}^\top / \|\mathbf{r}\|^2$ is a projector onto the orthogonal complement of the subspace spanned by \mathbf{r} . The term \mathbf{c}_{12}^\top is isolated as the only component that depends on ${}^B \xi_s^{n+1}$ via ${}^B \mathbf{v}_s$, which implies that $\text{rank}(\Psi_2) = 1$ if $\mathbf{c}_{12} \neq \mathbf{0}$. Therefore,

$$\Psi \mathbf{E}^{-1} \Psi^\top = \sum_{i=1}^2 \sum_{j=1}^2 \Psi_i \mathbf{E}^{-1} \Psi_j^\top = \mathbf{D}_0 + \mathbf{D}, \quad (64)$$

where $\mathbf{D}_0 \triangleq \Psi_1 \mathbf{E}^{-1} \Psi_1^\top \succcurlyeq \mathbf{0}$, and $\mathbf{D} \triangleq \mathbf{D}_1 + \mathbf{D}_2 \triangleq \Psi_2 \mathbf{E}^{-1} (\Psi_1^\top + \Psi_2^\top) + \Psi_1 \mathbf{E}^{-1} \Psi_2^\top$ is a symmetric matrix. Since each term has rank 1 due to $\text{rank}(\Psi_2) = 1$, we have $\text{rank}(\mathbf{D}) \leq 1 + 1 = 2$, and $\text{rank}(\mathbf{D}) = 0$ or 2 . The matrix \mathbf{D} reads explicitly as

$$\mathbf{D} = \begin{bmatrix} \mathbf{0} & \mathbf{d} \\ \mathbf{d}^\top & d_0 \end{bmatrix}, \quad \mathbf{E}^{-1} = \begin{bmatrix} \mathbf{E}_{11} & \mathbf{E}_{12} \\ \mathbf{E}_{12}^\top & \mathbf{E}_{22} \end{bmatrix}, \quad (65)$$

where $\mathbf{d} = \mathbf{B} \mathbf{E}_{11} \mathbf{c}_{12}$, $d_0 = 2\mathbf{c}_{11}^\top \mathbf{E}_{11} \mathbf{c}_{12} + 2\mathbf{c}_2^\top \mathbf{E}_{21} \mathbf{c}_{12} + \mathbf{c}_{12}^\top \mathbf{E}_{11} \mathbf{c}_{12}$. If $\mathbf{c}_{12} \neq \mathbf{0}$, \mathbf{D} is indefinite and has rank 2 with its inertia as $(1, 1, 2)$, which can be proven via the characteristic equation $\det(\mathbf{D} - \lambda \mathbf{I}) = (-\lambda)^3 (d_0 - \lambda + \|\mathbf{d}\|^2 / \lambda) = 0$, implying one positive and one negative eigenvalue. By rewriting $\Psi_n \mathbf{E}^{-1} \Psi_n^\top$, we have

$$\mathbf{P}_2: \quad \min_{\xi_s^{n+1}} -\log \det \left(\tilde{\mathbf{A}}^{-1} + \mathbf{D}_0 + \mathbf{D} \right) \quad \text{s.t.} \quad (30), \quad (66)$$

where $\mathbf{D} = \mathbf{e}_4 \xi_s^{n+1, \top} \mathbf{K}^\top + \mathbf{K} \xi_s^{n+1} \mathbf{e}_4^\top + \xi_s^{n+1, \top} \tilde{\mathbf{P}} \xi_s^{n+1} \mathbf{e}_4 \mathbf{e}_4^\top$, $\mathbf{K} \triangleq \tilde{\mathbf{E}}^\top \mathbf{M} \mathbf{S}$, and $\tilde{\mathbf{P}} \triangleq \mathbf{S}^\top \mathbf{M}^\top \mathbf{E}_{11} \mathbf{M} \mathbf{S} \succcurlyeq \mathbf{0}$, and $\tilde{\mathbf{E}} \triangleq [\mathbf{E}_{11} \mathbf{B}^\top \quad \mathbf{E}_{11} \mathbf{c}_{11} + \mathbf{E}_{12} \mathbf{c}_2]$, $\mathbf{M} \triangleq -\frac{2f_c}{c\|\mathbf{r}\|} \cdot \mathbf{R}^\top \mathbf{P}_r^\perp$, $\mathbf{S} \triangleq [-[\mathbf{s}]_\times \quad \mathbf{I}]$.

B. Trajectory Optimization Formulation as (P₂)

Considering the sparsity of \mathbf{D} , the dimension of the problem can be further reduced by leveraging the determinant property of block matrices. By factorising $\tilde{\mathbf{A}}^{-1} + \mathbf{D}_0 \succcurlyeq \mathbf{0}$, we have

$$\tilde{\mathbf{A}}^{-1} + \mathbf{D}_0 \triangleq \begin{bmatrix} \tilde{\mathbf{A}} & \mathbf{a} \\ \mathbf{a}^\top & a_0 \end{bmatrix}, \quad (67)$$

whose determinant is given as $\det(\tilde{\mathbf{A}}^{-1} + \mathbf{D}_0) = \det(\tilde{\mathbf{A}}) \cdot (a_0 - \mathbf{a}^\top \tilde{\mathbf{A}}^{-1} \mathbf{a})$. Similarly, we have $\det(\tilde{\mathbf{A}}^{-1} + \mathbf{D}_0 + \mathbf{D}) = \det(\tilde{\mathbf{A}}) \cdot ((d_0 + a_0) - (\mathbf{d}^\top + \mathbf{a}^\top) \tilde{\mathbf{A}}^{-1} (\mathbf{d} + \mathbf{a}))$, from which $\det(\tilde{\mathbf{A}}^{-1} + \mathbf{D}_0)$ can be separated, i.e.,

$$\begin{aligned} \det(\tilde{\mathbf{A}}^{-1} + \mathbf{D}_0 + \mathbf{D}) &= \det(\tilde{\mathbf{A}}^{-1} + \mathbf{D}_0) + \det(\tilde{\mathbf{A}}) \cdot (d_0 - 2\mathbf{a}^\top \tilde{\mathbf{A}}^{-1} \mathbf{d} - \mathbf{d}^\top \tilde{\mathbf{A}}^{-1} \mathbf{d}) \\ &= \det(\tilde{\mathbf{A}}^{-1} + \mathbf{D}_0) \left(1 + c_0 \left(\mathbf{c}^\top \xi_s^{n+1} + \xi_s^{n+1, \top} \tilde{\mathbf{P}} \xi_s^{n+1} \right) \right), \end{aligned} \quad (68)$$

with

$$c_0 \triangleq \det(\tilde{\mathbf{A}}) / \det(\tilde{\mathbf{A}}^{-1} + \mathbf{D}_0) > 0, \quad (69)$$

$$\mathbf{c} \triangleq \mathbf{S}^\top \mathbf{M}^\top (\mathbf{E}_{11} \mathbf{c}_{11} + \mathbf{E}_{12} \mathbf{c}_2 - \mathbf{E}_{11} \mathbf{B}^\top \tilde{\mathbf{A}}^{-1} \mathbf{a}), \quad (70)$$

$$\begin{aligned} \tilde{\mathbf{P}} &\triangleq \tilde{\mathbf{P}} - \mathbf{S}^\top \mathbf{M}^\top \mathbf{E}_{11} \mathbf{B}^\top \tilde{\mathbf{A}}^{-1} \mathbf{B} \mathbf{E}_{11} \mathbf{M} \mathbf{S} \\ &= \mathbf{S}^\top \mathbf{M}^\top \mathbf{E}_{11}^{\frac{1}{2}} \left(\mathbf{I} - \mathbf{E}_{11}^{\frac{1}{2}} \mathbf{B}^\top \tilde{\mathbf{A}}^{-1} \mathbf{B} \mathbf{E}_{11}^{\frac{1}{2}} \right) \mathbf{E}_{11}^{\frac{1}{2}} \mathbf{M} \mathbf{S}. \end{aligned} \quad (71)$$

By substituting (67)-(71) into (66), we have

$$\min_{\xi_s^{n+1}} -\log \left(1 + c_0 \left(\xi_s^{n+1, \top} \bar{\mathbf{P}} \xi_s^{n+1} + 2\mathbf{c}^\top \xi_s^{n+1} \right) \right). \quad (72)$$

Since $\tilde{\mathbf{A}}^{-1} + \mathbf{D}_0 + \mathbf{D} \succ \mathbf{0}$, and $\tilde{\mathbf{A}}^{-1} + \mathbf{D}_0 \succ \mathbf{0}$, the logarithm's argument is positive. Thus, the objective function becomes maximizing $\xi_s^{n+1, \top} \bar{\mathbf{P}} \xi_s^{n+1} + 2\mathbf{c}^\top \xi_s^{n+1}$, i.e.,

$$\mathbf{P}'_2 : \max_{\xi_s^{n+1}} \xi_s^{n+1, \top} \bar{\mathbf{P}} \xi_s^{n+1} + 2\mathbf{c}^\top \xi_s^{n+1}, \quad \text{s.t.} \quad (30). \quad (73)$$

REFERENCES

[1] K. Meng, Q. Wu, S. Ma, W. Chen, and T. Q. Quek, "Uav trajectory and beamforming optimization for integrated periodic sensing and communication," *IEEE Wireless Communications Letters*, vol. 11, no. 6, pp. 1211–1215, 2022.

[2] Z. Lyu, G. Zhu, and J. Xu, "Joint maneuver and beamforming design for uav-enabled integrated sensing and communication," *IEEE Transactions on Wireless Communications*, vol. 22, no. 4, pp. 2424–2440, 2022.

[3] X. Jing, F. Liu, C. Masouros, and Y. Zeng, "Isac from the sky: Uav trajectory design for joint communication and target localization," *IEEE Transactions on Wireless Communications*, 2024.

[4] J. Wu, W. Yuan, and L. Bai, "On the interplay between sensing and communications for uav trajectory design," *IEEE Internet of Things Journal*, vol. 10, no. 23, pp. 20383–20395, 2023.

[5] K. Meng, Q. Wu, S. Ma, W. Chen, K. Wang, and J. Li, "Throughput maximization for uav-enabled integrated periodic sensing and communication," *IEEE Transactions on Wireless Communications*, vol. 22, no. 1, pp. 671–687, 2022.

[6] F. Dong, F. Liu, Y. Cui, W. Wang, K. Han, and Z. Wang, "Sensing as a service in 6g perceptive networks: A unified framework for isac resource allocation," *IEEE Transactions on Wireless Communications*, vol. 22, no. 5, pp. 3522–3536, 2022.

[7] F. Liu, W. Yuan, C. Masouros, and J. Yuan, "Radar-assisted predictive beamforming for vehicular links: Communication served by sensing," *IEEE Transactions on Wireless Communications*, vol. 19, no. 11, pp. 7704–7719, 2020.

[8] F. Liu, Y.-F. Liu, A. Li, C. Masouros, and Y. C. Eldar, "Cramér-rao bound optimization for joint radar-communication beamforming," *IEEE Transactions on Signal Processing*, vol. 70, pp. 240–253, 2021.

[9] X. Li, V. C. Andrei, U. J. Mönich, and H. Boche, "Optimal and robust waveform design for mimo-ofdm channel sensing: A cramér-rao bound perspective," in *ICC 2023-IEEE International Conference on Communications*. IEEE, 2023, pp. 3516–3521.

[10] K. M. Braun, "Ofdm radar algorithms in mobile communication networks," Ph.D. dissertation, Karlsruhe, Karlsruher Institut für Technologie (KIT), Diss., 2014, 2014.

[11] D. Tse and P. Viswanath, *Fundamentals of Wireless Communication*. Cambridge University Press, 2005.

[12] A. Mueller, "Modern robotics: Mechanics, planning, and control [bookshelf]," *IEEE Control Systems Magazine*, vol. 39, no. 6, pp. 100–102, 2019.

[13] E. Gallo, "The so (3) and se (3) lie algebras of rigid body rotations and motions and their application to discrete integration, gradient descent optimization, and state estimation," *arXiv preprint arXiv:2205.12572*, 2022.

[14] J. Solà, J. Deray, and D. Atchuthan, "A micro Lie theory for state estimation in robotics," 2021.

[15] Y. Ma, S. Soatto, J. Košecká, and S. Sastry, *An invitation to 3-d vision: from images to geometric models*. Springer, 2004, vol. 26.

[16] H. V. Trees, K. Bell, and Z. Tian, *Detection estimation and modulation theory, part I: Detection, estimation, and filtering theory*, 2013, vol. 8, no. 10.

[17] C. Chahbazian, K. Dahia, N. Merlinge, B. Winter-Bonnet, A. Blanc, and C. Musso, "Recursive posterior Cramér–Rao lower bound on Lie groups," *Automatica*, vol. 160, p. 111422, 2024.

[18] B. C. Hall and B. C. Hall, *Lie groups, Lie algebras, and representations*. Springer, 2013.

[19] N. J. Higham, *Accuracy and stability of numerical algorithms*. SIAM, 2002.

[20] L. Zuo, R. Niu, and P. K. Varshney, "Conditional Posterior Cramér–Rao Lower Bounds for Nonlinear Sequential Bayesian Estimation," *IEEE Transactions on Signal Processing*, vol. 59, pp. 1–14, 2011.

[21] S. M. Kay, "Fundamentals of statistical signal processing: Estimation theory," 1993.

[22] J. Li, L. Xu, P. Stoica, K. W. Forsythe, and D. W. Bliss, "Range compression and waveform optimization for mimo radar: A cramér-rao bound based study," *IEEE Transactions on Signal Processing*, vol. 56, no. 1, pp. 218–232, 2007.

[23] H. Zhang, B. Zong, and J. Xie, "Power and bandwidth allocation for multi-target tracking in collocated mimo radar," *IEEE Transactions on Vehicular Technology*, vol. 69, no. 9, pp. 9795–9806, 2020.

[24] F. Zhang, *The Schur complement and its applications*. Springer Science & Business Media, 2006, vol. 4.